JOURNAL OF Materials CHEMISTRY

Use of ethylene oxide in the sol–gel synthesis of α-Fe_2O_3 nanoparticles from Fe(III) salts

Wenting Dong*† and Congshan Zhu

Photon Craft Project Lab, Shanghai Institute of Optics and Fine Mechanics, Chinese Academy of Sciences, P.O. Box 800-211, Shanghai 201800, P. R. China.
E-mail: dong@mpi-muelheim.mpg.de

Received 21st January 2002, Accepted 14th March 2002
First published as an Advance Article on the web 11th April 2002

α-Fe_2O_3 nanoparticles were prepared by the sol–gel process with ethylene oxide (EO) and $FeCl_3$ as starting materials. The influences of the molar ratio of EO to Cl^-, the concentration of $FeCl_3$, the volume percentage of ethanol and heat treatment on the structural properties of the α-Fe_2O_3 nanoparticles were investigated by XRD, TEM and SAXS (small angle X-ray scattering) techniques. It was found that the mean size of the α-Fe_2O_3 nanoparticles formed *via* the sol–gel process is smaller than those formed *via* the sol process. The values of the mass fractal dimension (D_m) for the α-Fe_2O_3 nanoparticles formed *via* the sol and sol–gel processes are $2 < D_m < 3$ and $3 < D_m < 4$, respectively.

1 Introduction

α-Fe_2O_3 (hematite) nanoparticles have attracted great attention in recent years because of their wide applications in the areas of pigments, catalysts,[1] nonlinear optics,[2] gas sensors[3] and so on. Considerable efforts have been made in the development of synthetic approaches to iron oxide nanoparticles, such as chemical precipitation,[4,5] forced hydrolysis,[6,7] the microemulsion technique,[8] sol–gel processes,[3,9] *etc.*[10–12] The sol–gel and chemical precipitation methods are widely used in preparing high yields of α-Fe_2O_3 nanoparticles using an inorganic iron salt and base as starting materials. However, it was reported that it is difficult to wash the alkali out of the precipitate if the base is an alkali hydroxide.[13] Furthermore, if ammonium hydroxide is used, contamination by the anion of the iron salt cannot be avoided. Moreover, the hydroxide or metal oxide nanoparticles will aggregate if attempts are made to get rid of the contamination by washing.

In our new method, a simple chemical precipitation approach *via* a sol–gel process was successfully employed to synthesize α-Fe_2O_3 nanoparticles without the problems of contamination and aggregation mentioned above.[14] α-Fe_2O_3 nanoparticles were prepared by using ethylene oxide (EO) and $FeCl_3$ as starting materials. Two communications have reported the use of ethylene oxide or epichlorohydrin and $ZrOCl_2$ as starting materials to produce ZrO_2 nanoparticles.[15,16] In addition, propylene oxide was used as a gelation agent to prepare porous iron oxide monoliths from Fe(III) salts.[17] In these papers, epoxides were very effective in the synthesis of metal oxide nanoparticles or monoliths *via* sol–gel processes with inorganic salts as precursors. In this full paper, we will investigate the details of the influences of different preparation conditions on the formation of α-Fe_2O_3 nanoparticles by XRD, TEM and small angle X-ray scattering (SAXS) techniques.

2 Experimental

The principle of the formation of α-Fe_2O_3 nanoparticles has been briefly introduced elsewhere[14] and it will be described in detail in this paper. In this work, EO and $FeCl_3$ were used as the precursors to produce α-Fe_2O_3 nanoparticles. EO was selected as one of the starting materials because it reacts readily with HCl, one of the hydrolysis products of $FeCl_3$. It is already known that a hydrolysis equilibrium exists in the aqueous $FeCl_3$ solution:

$$FeCl_3 + 3\ H_2O \rightarrow Fe(OH)_3 + 3\ HCl\ \text{(hydrolysis)} \quad (1.1)$$

and α-Fe_2O_3 particles will form through a two-step phase transformation:[18,19]

$$Fe(OH)_3 \rightarrow \beta\text{-FeOOH} \rightarrow \alpha\text{-}Fe_2O_3\ \text{(phase transformation)} \quad (1.2)$$

If C_2H_4O (EO) is added to the above system, the reactions illustrated below will take place.[14–16,20,21]

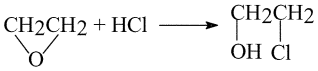

(2)

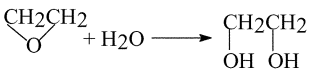

(3)

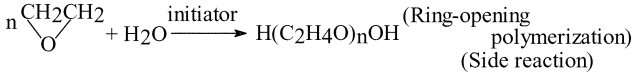

(4)

It can be seen from the reactions (2)–(4) that the ionic strength of the reaction system decreases during the whole reaction process and $Fe(OH)_3$ sol or gel will form *via* association and polymerization. It was reported that β-FeOOH loses its structural water and is completely transformed to α-Fe_2O_3 within the temperature range of 235 to 275 °C with an exothermic effect.[3] The products of reactions (2) and (3) can be driven out at 200 °C because the melting points of $(HO)CH_2CH_2Cl$ and $CH_2CH_2(OH)_2$ are 128.6 and 197.6 °C, respectively. It can be seen from reaction (4) that ring-opening polymerization of EO may also take place with $FeCl_3$ as a catalyst[20] or with iron alkoxide as an initiator, which can be formed by reaction of ethylene glycol with $FeCl_3$ or of EO with $FeCl_3$.[21] However, the

†*Current address*: Max-Planck-Institut für Kohlenforschung, Kaiser-Wilhelm-Platz 1, 45470 Mülheim an der Ruhr, Germany.

 DOI: 10.1039/b200773h

likelihood of this reaction is low because of the large amount of H_2O in the reaction system. The possible by-product, $H(C_2H_4O)_nOH$ (polyethylene glycol, PEG), will have an effect on preventing the $Fe(OH)_3$ nanoparticles from agglomerating. Therefore, uniform α-Fe_2O_3 nanoparticles will be obtained after aging and heating at 200 °C to drive out the by-products and at 300 °C to complete the phase transformation.

The preparation procedure can be described briefly as follows.[14] The starting materials were analytical reagent-grade $FeCl_3$, EO and C_2H_5OH (EtOH). **CAUTION**: *EO is an explosive, flammable, carcinogenic, and toxic chemical and should be handled very carefully. It should be stored in a refrigerator. All of the following operations were carried out in a well-ventilated chemical fume hood. Spectacles and gloves are needed for protection.* First, an aqueous solution of $FeCl_3$ and a mixture of EO and EtOH were put into the ice bath and cooled respectively. Then a mixture of EO and EtOH was dropped slowly into the aqueous solution of $FeCl_3$. A red–brown sol formed first for all the samples, and some of the sol later became gel. The sols and gels were heated at 200 °C to drive out the by-products. After heating at 300 °C, nanoparticles of Fe_2O_3 were obtained. In this paper, α-Fe_2O_3 nanoparticles were prepared by using different preparation conditions, *i.e.*, variation in the molar ratio of EO to Cl^-, the concentration of Fe^{3+}, the amount of ethanol and the calcination temperature. The experimental conditions are listed in Table 1.

The XRD measurements were carried out with a Rigaku D/max-rA rotation anode X-ray diffractometer. The TEM measurements were obtained by means of a JEOL-JEM-200CX transmission electronic microscope. The mean particle sizes of the α-Fe_2O_3 nanoparticles were calculated by statistical analysis of 100 particles in the field of the TEM views. The average size, d_{TEM}, is calculated by the arithmetic mean value of the sizes of these particles, *i.e.*, $d_{TEM} = \sum_{i=1}^{100} d_i/100$, where d_i is the size of one particle.[22] SAXS measurements were carried out at the SAXS station at the Beijing Synchrotron Radiation Laboratory (BSRL) in the Beijing Electron Positron Collider National Laboratory (BEPC NL). The samples were ground into fine powders and sprinkled on adhesive cellophane tape. The dependence of the scattering intensity on the angle was measured. The main components of the SAXS set-up have been described elsewhere.[23] The SAXS intensity $I(q)$ (where q is the modulus of the scattering wave vector) was corrected for incident intensity variation, sample thickness, transmission and background scattering before data fitting could be achieved.

Table 1 Summary of the different conditions used for the preparation of α-Fe_2O_3 nanoparticles

(a) Prepared with different initial concentrations of $FeCl_3$[a]

Sample	C_{FeCl_3}[a]/mol l^{-1}	Sol–gel process
1	0.05	Gel not formed (sol)
2	0.1	Gel not formed (sol)
3	0.3	Gel formed after 17 h
4	1	Gel formed after 10 min
5	2	Gel formed after 3 min

(b) Prepared with different molar ratios of EO to Cl^-[b]

Sample	$Mol_{EO:Cl^-}$[b]	Sol–gel process
a	0.5	Gel not formed (sol)
b	1	Gel not formed (sol)
c	1.5	Gel formed after 28 h
d	2.5	Gel formed after 6 h
e	3	Gel formed after 4 h

(c) Prepared with different volume percentages of EtOH[c]

Sample	V_{EtOH}[c] (%)	Sol–gel process
A	25	Gel formed after 10 h
B	35	Gel formed after 14 h
C	45	Gel formed after 20 h
D	55	Gel not formed (sol)

(d) Prepared with different heating temperatures[d]

Sample	Heat treatment
I	300 °C, 3 h
II	450 °C, 3 h
III	700 °C, 3 h

[a]The molar ratio of EO to Cl^- is 2.5 and the volume percentage of EtOH is 15%. C_{FeCl_3} = concentration of $FeCl_3$. [b]The concentration of $FeCl_3$ is 0.5 M and the volume percentage of EtOH is 15%. $Mol_{EO:Cl^-}$ = molar ratio of EO to Cl^-. [c]The molar ratio of EO to Cl^- is 2.25 and the concentration of $FeCl_3$ is 0.5 M. V_{EtOH} = volume percentage of EtOH. [d]The molar ratio of EO to Cl^- is 2.25, the concentration of $FeCl_3$ is 0.5 M and the volume percentage of EtOH is 45%.

3 Results

3.1 Powder X-ray diffraction

The XRD patterns of the Fe_2O_3 nanoparticles prepared with different volume percentages of EtOH are shown in Fig. 1. The XRD profiles of the Fe_2O_3 nanoparticles prepared under other conditions are nearly the same as those in Fig. 1, except for their peak widths. All of the prepared samples were indexed as pure α-Fe_2O_3 because the diffraction peaks of all the samples with lattice spacings of 3.68 (012), 2.70 (104), 2.52 (110), 2.20 (113), 1.84 (024) and 1.69 Å (116) are in agreement with those in JCPDS Card No.33-664, which indicates the standard XRD pattern of α-Fe_2O_3. The average particle size (D_{hkl}) was calculated by using the Debye–Scherrer equation[24] (in this paper, $K = 0.89$ because β_{size} was defined as FWHM of the diffraction peak). The calculated D_{104} values and lattice constants are shown in Tables 3–6.

3.2 TEM pictures

Fig. 2 shows the TEM pictures and selected diffraction patterns of α-Fe_2O_3 nanoparticles prepared with different molar ratios of C_2H_4O to Cl^-. From the electron diffraction patterns of samples a, b and c, it can seen that the crystallinity of the α-Fe_2O_3 nanoparticles increases with increasing molar ratio. There was a noticeable degree of particle coarsening in samples a and b, but the morphology of sample c became uniform. Table 2 shows the results of local quantitative analysis of the α-Fe_2O_3 nanoparticles prepared from different molar ratios of EO to Cl^-. It demonstrates that the molar ratio of O to Fe in

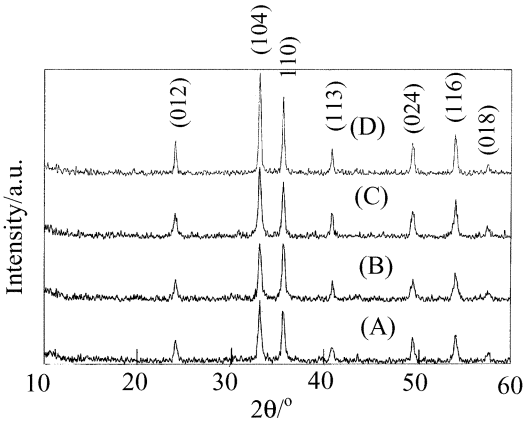

Fig. 1 XRD patterns of Fe_2O_3 nanoparticles prepared with different volume percentages of EtOH.

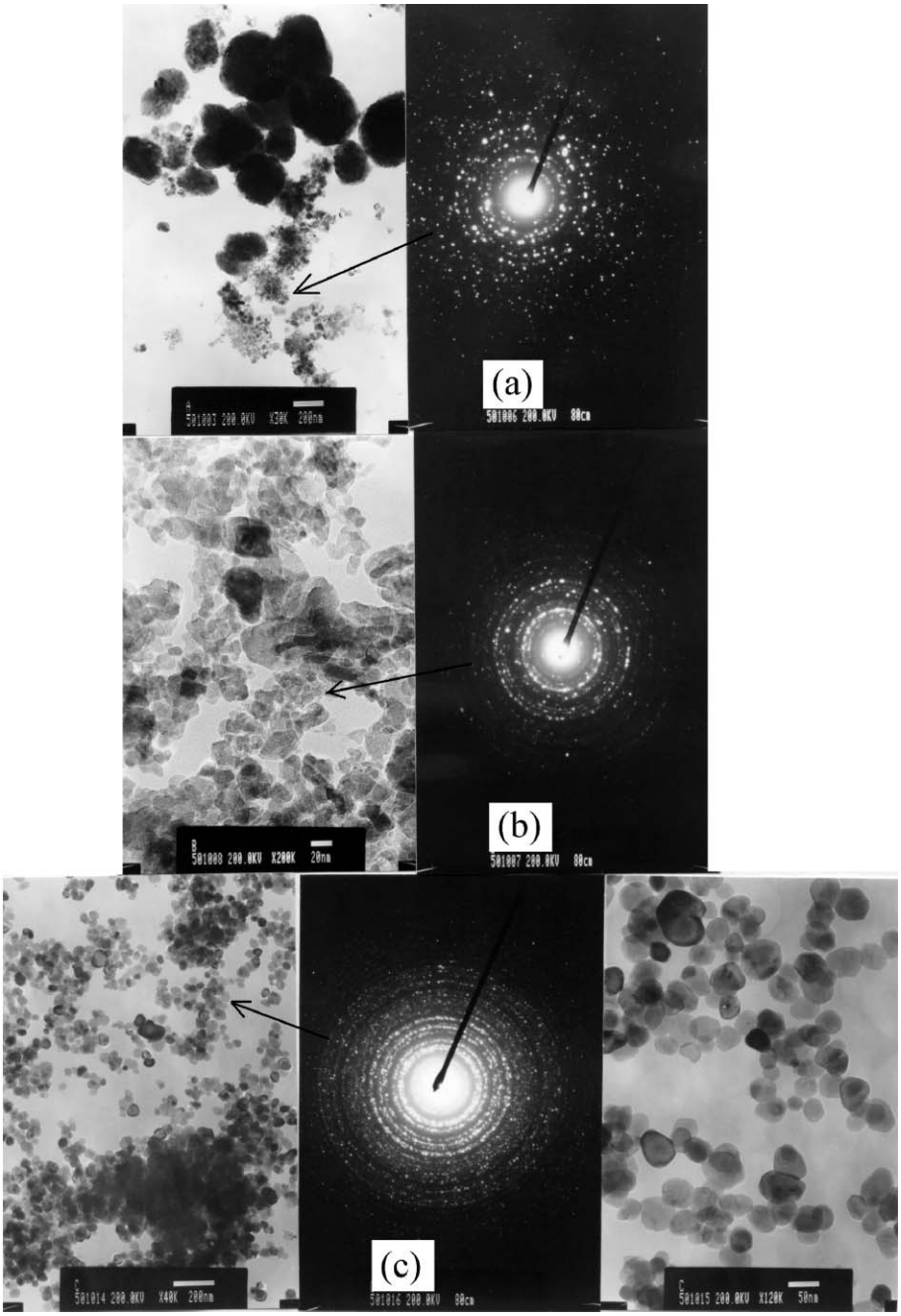

Fig. 2 TEM view of α-Fe_2O_3 nanoparticles prepared with different molar ratios of EO to Cl^-.

the α-Fe_2O_3 particles is close to 1.5 if the molar ratio of EO to Cl^- is larger than 1, indicating that α-Fe_2O_3 has been formed. This implies that it is crucial to set the molar ratio of EO to Cl^- to be more than 1.5 in order to get α-Fe_2O_3 nanoparticles with good morphology and crystallinity.

Fig. 3 shows the bright field TEM of α-Fe_2O_3 nanoparticles prepared with different initial concentrations of $FeCl_3$. It can be seen that initial concentrations of 0.05 and 0.1 M do not result in good morphology of the α-Fe_2O_3 nanoparticles and indicate aggregation of the particles. However, small and uniform α-Fe_2O_3 nanoparticles form when the initial concentration of $FeCl_3$ is not less 0.3 M.

It is also found that the size of the α-Fe_2O_3 nanoparticles increases with increasing heating temperature. Fig. 4 shows the TEM pictures of α-Fe_2O_3 nanoparticles calcined at 700 °C and it can be seen that some of the particles change their shape to spindle.

Table 2 Results of local quantitative analysis of the α-Fe_2O_3 particles prepared with different molar ratios of EO to Cl^-[a]

Sample	Molar ratio of C_2H_4O to Cl^-	Fe content (mol%)	O content (mol%)	Molar ratio of O and Fe
a	0.5	36.87	63.13	1.39
b	1	40.79	59.21	1.45
c	1.5	41.88	58.12	1.59

[a]The detected area of X-ray energy dispersive spectrometry (XEDS) is indicated by the arrows in Fig. 2.

3.3 Small angle X-ray scattering

Fig. 5 shows the SAXS profiles of α-Fe_2O_3 nanoparticles prepared under different conditions. The scattering intensity $I(q)$ is plotted as a function of the scattering vector q, which is defined as $q = 4\pi\sin\theta/\lambda$, in which θ is half the scattering angle and λ is the wavelength of the incident X-ray beam (in this paper, $\lambda = 1.54$ Å). It can be seen that all the SAXS profiles of the α-Fe_2O_3 nanoparticles are similar and their shapes can

Table 3 Structural data of α-Fe_2O_3 nanoparticles prepared from different molar ratios of EO to Cl^-[a]

			Mean particle size/nm					
	Lattice constant (by XRD)			SAXS		R_g/nm		
Sample	*a*/Å	*c*/Å	XRD D_{104}	d^{large}	d^{small}	R_g^{large}	R_g^{small}	D_m
a	5.038	13.757	37.5	27.1	4.5	10.5	1.7	2.64
b	5.040	13.770	45.5	38.0	8.1	14.6	3.2	2.63
c	5.046	13.826	31.5	30.9	6.7	12.0	2.6	3.59
d	5.044	13.763	31.4	26.0	6.5	10.1	2.5	3.24
e	5.042	13.762	31.2	24.5	6.0	9.5	2.3	3.43

[a]The concentration of $FeCl_3$ is 0.5 M and the volume percentage of EtOH is 15%; R_g = radius of gyration; D_m = mass fractal dimension; D_{104} = length of particles perpendicular to the (104) crystal plane.

Table 4 Structural data of the α-Fe_2O_3 nanoparticles prepared with different initial concentrations of $FeCl_3$[a]

			Mean particle size /nm						
	Lattice constant (by XRD)				SAXS		R_g/nm		
Sample	a(Å)	c(Å)	XRD D_{104}	TEM D_{TEM}	d^{large}	d^{small}	R_g^{large}	R_g^{small}	D_m
1	5.038	13.757	35.5	—	30.6	6.2	11.8	2.4	2.86
2	5.036	13.777	49.7	—	34.2	6.2	13.3	2.4	2.62
3	5.046	13.727	24.6	32.0	30.0	6.3	12.0	2.4	3.50
4	5.040	13.803	23.2	29.5	28.7	6.1	11.3	2.4	3.84
5	5.042	13.734	19.7	24.7	25.3	6.4	9.8	2.5	3.91

[a]The molar ratio of EO to Cl^- is 2.5 and the volume percentage of EtOH is 15%; C_{FeCl_3} = concentration of $FeCl_3$; R_g = radius of gyration; D_m = mass fractal dimension; D_{104} = length of particles perpendicular to the (104) crystal plane; D_{TEM} = mean particle size of 100 particles calculated from the TEM views in Fig. 3; D_{TEM} of samples 1 and 2 could not be obtained because of their obscured TEM views.

Table 5 Structural data of α-Fe_2O_3 nanoparticles prepared with different volume percentages of EtOH[a]

			Mean particle size/nm						
	Lattice constant (by XRD)				SAXS		R_g/nm		
Sample	*a*/Å	*c*/Å	XRD D_{104}	TEM D_{TEM}	d^{large}	d^{small}	R_g^{large}	R_g^{small}	D_m
A	5.032	13.762	31.2	32.8	32.0	7.2	12.4	2.8	3.58
B	5.036	13.752	22.4	28.9	27.3	6.5	10.6	2.5	3.70
C	5.042	13.742	24.5	30.1	29.3	6.6	11.3	2.6	3.53
D	5.034	13.756	45.0	50.6	32.6	6.6	12.6	2.6	3.58

[a]The molar ratio of EO to Cl^- is 2.25 and the concentration of $FeCl_3$ is 0.5 M; V_{EtOH} = volume percentage of EtOH; R_g = radius of gyration; D_m = mass fractal dimension. D_{104} = length of particles perpendicular to the (104) crystal plane; D_{TEM} = mean particle size of 100 particles calculated from the TEM views in Fig. 2 of ref. 14.

Table 6 SAXS data of the α-Fe_2O_3 nanoparticles prepared at different heating temperatures[a]

			Mean particle size/nm					
	Lattice constant (by XRD)			SAXS		R_g/nm		
Sample	*a*/Å	*c*Å	XRD D_{104}	d^{large}	d^{small}	R_g^{large}	R_g^{small}	D_m
I	5.024	13.742	24.5	29.3	6.6	11.3	2.6	3.53
II	5.038	13.774	41.5	36.1	6.5	14.0	2.6	3.64
III	5.032	13.726	64.0	52.0	6.4	20.1	2.5	3.38

[a]The molar ratio of EO to Cl^- is 2.25 , the concentration of $FeCl_3$ is 0.5 M and the percentage of EtOH is 45%; R_g = radius of gyration; D_m = mass fractal dimension; D_{104} = length of particles perpendicular to the (104) crystal plane.

be described by monotonically decreasing curves. They show a general trend that the intensity decreases with increasing q until a constant minimum value of $I(q)$ is reached.

In this single-phase α-Fe_2O_3 nanoparticle system, the SAXS is mainly caused by the difference in the electron density within and around the nanoparticles. Using the Guinier approximation[25] (the scattering intensity in the very low q range is of Gaussian form and independent of the particles' shape), the radius of gyration, R_g, can be calculated from the Guinier plot [a plot of $I(q)$ *vs.* q^2] shown in Fig. 6. The curvature in the very low q region of the Guinier plot indicates that the α-Fe_2O_3 nanoparticles are polydispersed so that particle size determination by Guinier's law becomes problematic. However, we may estimate the size range of the particles in a polydispersed system because large particles dominate the scattering at low q and small particles dominate at high q.[26] Therefore, the sizes of large-end and small-end particles can be determined by the slopes of the Guinier plot in the low q (R_g^{large}) and high q regions (R_g^{small}), respectively. The results are listed in Tables 3–6.

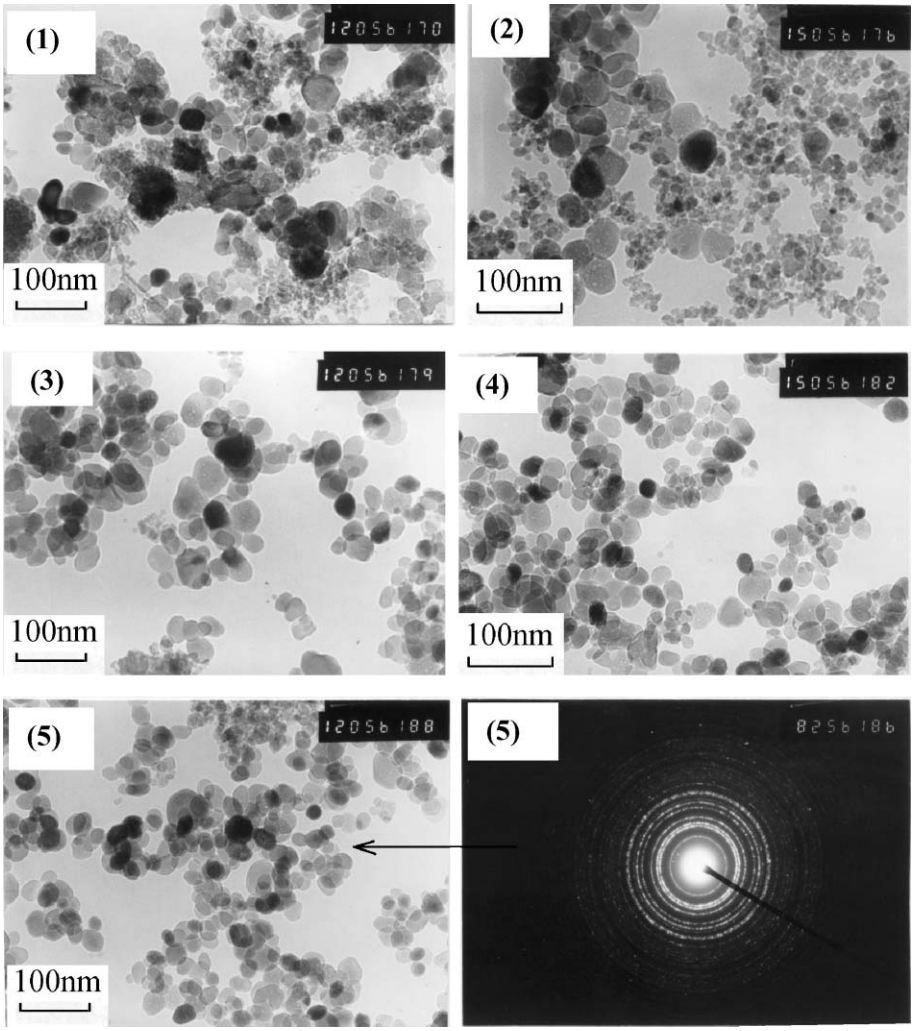

Fig. 3 TEM view of α-Fe_2O_3 nanoparticles prepared with different initial concentrations of $FeCl_3$.

In some cases, aggregation of the particles can be connected *via* a network, which displays "fractal-like" properties in the middle length scale region that is between $qR_g > 1$ and $qa < 1$, where a is the sub-element or base unit length of the fractal object. Mass fractal dimension (D_m) is usually used to describe various disordered systems, such as sol–gel materials, and it can semiquantitatively characterize the surface roughness and structure density of polymerized particles.[27] In this region, the intensity profile can be approximated to a very simple power-law relationship, $I(q) \propto q^{D_m}$, where D_m is the mass fractal dimension. Therefore, the value of the fractal dimension corresponds to a certain structure or indicates a certain type of network growth. Fig. 7 shows the curves of ln $I(q)$ *vs.* ln q and the calculated D_m values are listed in Tables 3–6.

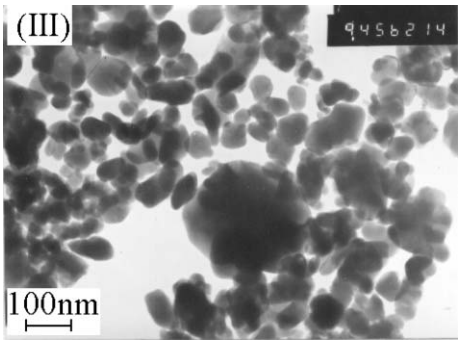

Fig. 4 TEM view of α-Fe_2O_3 nanoparticles calcined at 700 °C.

4 Discussion

The collected structural data shed light on the formation of α-Fe_2O_3 nanoparticles by the sol–gel process with $FeCl_3$ and EO as starting materials. The particle sizes calculated by SAXS and XRD both rely on the assumption that the shape of the particles is spherical. However, the mean sizes of the particles calculated by these two methods show a small difference and this disagreement probably results from the difference in the measuring mechanism of the two methods. The D_{104} calculated by XRD is the length of the grain perpendicular to crystal plane (104) while the d^{large} calculated by SAXS is based on the Guinier radius R_g, *i.e.* the root-mean-square distance of all the scattering elements/electrons from the center of gravity. In spite of these differences, both D_{104} and d^{large} show similar trends. R_g^{large} in Tables 3–6 varies with the different preparative conditions while the value of R_g^{small} does not show much variation for all the samples. The constant occurrence of the small oligomeric species (R_g^{small} is between 17 and 32 Å) in all the samples indicates that the reactive consumption of small polymeric species is a rather slow kinetic process under all of the preparative conditions. The lattice constants of the α-Fe_2O_3 nanoparticles are also different from those of bulk α-Fe_2O_3. The reported lattice parameters of the pure rhombohedral hematite α-Fe_2O_3 are $a = 5.036$ and $c = 13.749$ Å. However, the a values of the prepared α-Fe_2O_3 nanoparticles vary slightly from 5.032 to 5.046 Å and the c values vary form 13.742 to 13.826 Å.

It can be seen from Tables 3 and 4 that both the molar ratio of EO to Cl^- ($mol_{EO:Cl^-}$) and the initial concentration of $FeCl_3$

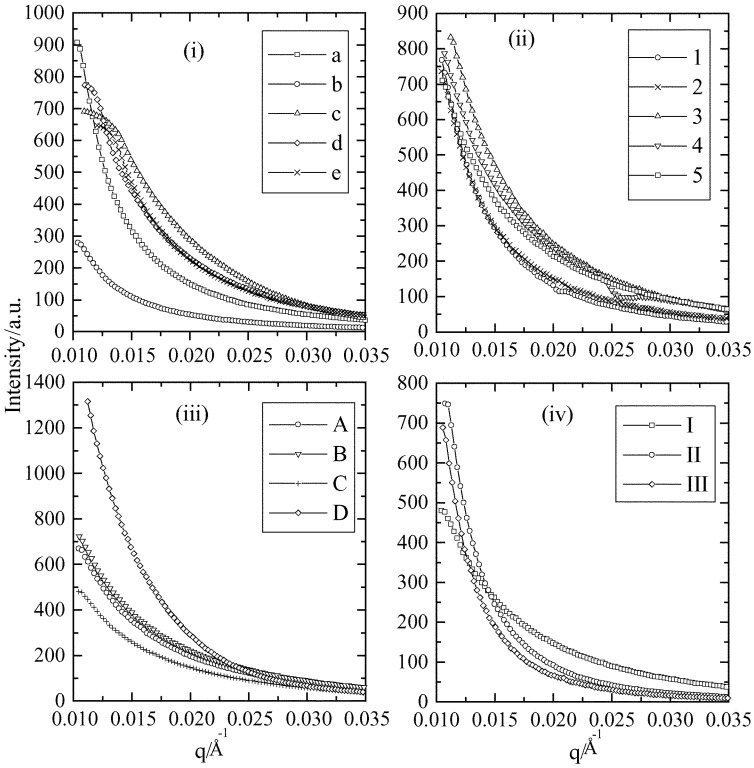

Fig. 5 SAXS profiles of α-Fe_2O_3 nanoparticles prepared under different experimental conditions: (i) different molar ratios of EO to Cl^-; (ii) different initial concentrations of $FeCl_3$; (iii) different volume percentages of EtOH; (iv) different heating temperatures.

(C_{FeCl_3}) play an important role in the formation of the α-Fe_2O_3 nanoparticles. If $mol_{EO:Cl^-}$ is less than 1 or C_{FeCl_3} is less than 0.1 M (the other reaction conditions can be seen in the footnotes of Tables 3 and 4), then a sol forms and the particle size increases with increasing $mol_{EO:Cl^-}$ or C_{FeCl_3}; while if $mol_{EO:Cl^-}$ is more than 1.5 or C_{FeCl_3} more than 0.3 M, a gel forms and the particle size decreases with increasing $mol_{EO:Cl^-}$ or C_{FeCl_3}. In addition, it can be estimated from the D_m values in Tables 3 and 4 ($2 < D_m < 3$) that the α-Fe_2O_3 nanoparticles formed *via* the sol process show surface roughness and grow like a mass fractal with connected structures. However, we can estimate from the D_m values in the tables ($3 < D_m < 4$) that the α-Fe_2O_3 nanoparticles formed *via* the sol–gel process possess smooth surfaces.

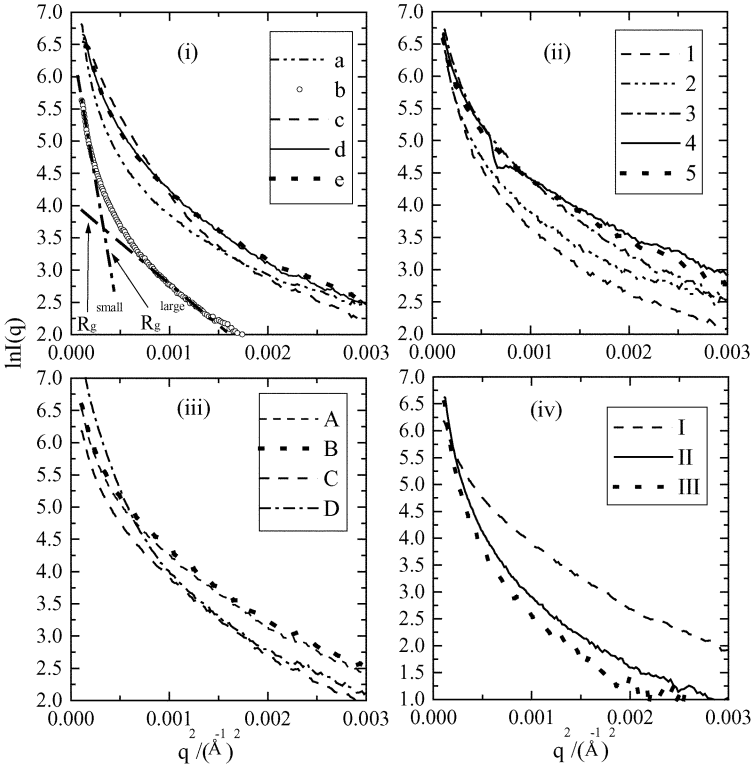

Fig. 6 Guinier plots of α-Fe_2O_3 nanoparticles prepared under different experimental conditions: (i) different molar ratios of EO to Cl^-; (ii) different initial concentrations of $FeCl_3$; (iii) different volume percentages of EtOH; (iv) different heating temperatures.

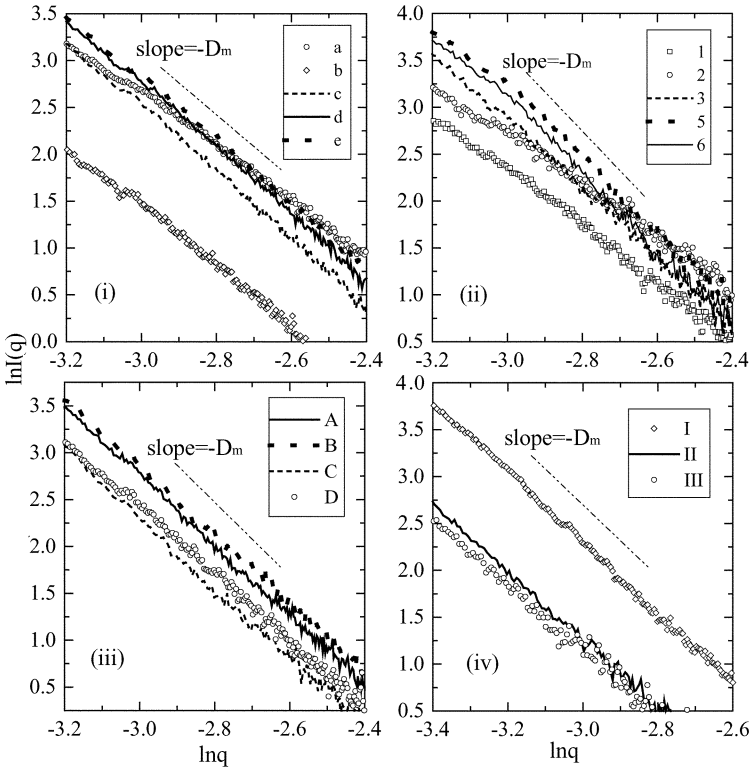

Fig. 7 ln $I(q)$ *vs.* ln q plots of α-Fe_2O_3 nanoparticles prepared under different experimental conditions: (i) different molar ratios of EO to Cl^-; (ii) different initial concentrations of $FeCl_3$; (iii) different volume percentages of EtOH; (iv) different heating temperatures.

The effect of EtOH on the formation of α-Fe_2O_3 nanoparticles has also been investigated. It can be estimated from Table 5 ($3 < D_m < 4$) that α-Fe_2O_3 nanoparticles with smooth surfaces are obtained, regardless of whether the particles are formed *via* a sol or sol–gel process. It was also found that if the volume percentage of EtOH (V_{EtOH}) is less than 45% (samples A, B, C), a gel will form. However, if V_{EtOH} is increased up to 55% (sample D), a gel will not form and the particle size becomes much larger than those formed *via* the gel process.

To the best of our knowledge, so far, only a few investigations have been reported on the interactions of ferric ions with lower alcohols or on the precipitation of ferric (hydrous) oxides in alcohol–water media.[28–30] It has been reported that hydrolysis and chloride complexation of ferric ions are enhanced in the presence of ethanol. These complexes are known to be precursors in the formation of β-FeOOH. Therefore, the first effect of EtOH could be to increase the concentration of Fe^{3+} or OH^- and enhance the hydrolysis of Fe^{3+}. In addition, another reaction also takes place as soon as EO is added to the reaction system that is abundant in EtOH:[31]

$$\underset{\diagdown\,O\,\diagup}{CH_2CH_2} + HO\text{-}C_2H_5 \xrightarrow{H^+} HO\text{-}CH_2CH_2\text{-}OC_2H_5$$

Therefore, less HCl will be consumed by EO because of the above competitive reaction and this effect can be regarded as inhibition of the hydrolysis of Fe^{3+}. Therefore, the addition of EtOH has two contrasting effects on the reaction of the system and the particle size is the net result of these effects. However, there are also indications that ferric ions may complex with ethanol,[32] although no chelation could be detected.[33] In addition, it was found that ethanol affects the rate and the mechanism of precipitation and of aging of β-FeOOH.[33] EtOH also exerts a profound effect on the morphology of ferric oxide.[30] Therefore, the influence of EtOH on the formation process is very complicated and further investigation is necessary.

The influence of heat treatment on the particle size was also investigated and the results are listed in Table 6. It can be estimated that α-Fe_2O_3 nanoparticles with smooth surfaces are formed ($3 < D_m < 4$) and the mean particle size increases with increasing temperature.

We also used this sol–gel method to prepare SnO_2, In_2O_3, ZnO, Bi_2O_3 and CdO semiconductor nanoparticles with their corresponding inorganic metal salts and EO as starting materials. The results showed that a similar sol–gel process took place in the formation of the SnO_2 and In_2O_3 nanoparticles while the sol–gel process did not take place during the formation of the ZnO, Bi_2O_3 and CdO nanoparticles. In addition, this method is also very useful for preparing Fe_2O_3, SnO_2 and In_2O_3 thin films by means of the sol–gel process by dip-coating or spin-coating methods. Investigations in these areas are under way in our group.

5 Conclusions

α-Fe_2O_3 nanoparticles with a particle size of between 20 and 60 nm were prepared by the sol–gel process with ethylene oxide and $FeCl_3$ as starting materials. The XRD, TEM and SAXS techniques were applied in order to investigate the properties of the α-Fe_2O_3 nanoparticles, including particle size and mass fractal dimension. The trends in the variation of particle size of the α-Fe_2O_3 nanoparticles determined by SAXS are in agreement with those found by XRD and TEM.

The mean particle size of the α-Fe_2O_3 nanoparticles formed *via* the sol process increases with increasing molar ratio of EO to Cl^- or with increasing concentration of $FeCl_3$ (in the range $mol_{EO:Cl^-} \leqslant 1$ or $C_{FeCl_3} \leqslant 0.1$ M). However, the size of the α-Fe_2O_3 nanoparticles formed *via* the sol–gel process decreases with increasing molar ratio of EO to Cl^- or with increasing concentration of $FeCl_3$ (in the range $mol_{EO:Cl^-} \geqslant 1.5$ or $C_{FeCl_3} \geqslant 0.3$ M). The particle size is also influenced by the volume percentage of ethanol present in the reaction system. The size of the α-Fe_2O_3 nanoparticles formed *via* the sol process ($V_{EtOH} \geqslant 55\%$) is larger than that of those formed *via* the

sol–gel process ($V_{EtOH} \leqslant 45\%$). Heat treatment also plays an important role in the size of the α-Fe_2O_3 nanoparticles. The higher the temperature used, the larger the particle size will be.

SAXS analyses also demonstrate that the fractal dimensions of the α-Fe_2O_3 nanoparticles are mainly determined by the molar ratio of EO to Cl^- or initial concentrations of $FeCl_3$. It is estimated that α-Fe_2O_3 nanoparticles with rough surfaces are formed *via* the sol process ($2 < D_m < 3$). In contrast, the D_m values of those formed *via* the sol–gel process are between 3 and 4, indicating the formation of α-Fe_2O_3 nanoparticles with smooth surfaces. However, the D_m values of α-Fe_2O_3 nanoparticles formed in the presence of EtOH or by heat treatment are also between 3 and 4, indicating the formation of α-Fe_2O_3 nanoparticles with smooth surfaces.

Acknowledgement

The authors of this paper would like to thank Professor Baozhong Dong, Dr Zhanghua Wu, Dr Yi Liu, and Dr Yongfan Ding, working at the SAXS station in the Beijing Synchrotron Radiation Laboratory, for their great help with our SAXS experiments and their beneficial discussions during the course of data processing. One of the authors, Wenting Dong, is very grateful to her colleagues, Dr Hongyan Jiang, Dr Cigang Xu, Dr Mingwen Tian, Dr Zaicheng Sun and Dr Meng He, for their helpful discussions on the mechanism of formation of the α-Fe_2O_3 nanoparticles. The authors also thank Dr Qinghua Zeng for his suggestions during the writing of this paper.

References

1 R. M. Cornell and U. Schwertmann, *The Iron Oxides*, VCH Verlagsgesellschaft, Weinheim, Germany, 1996, p. 463.
2 T. Hashimoto, T. Yoko and S. Saka, *J. Ceram. Soc. Jpn.*, 1993, **101**, 64.
3 X. Q. Liu, S. W. Tao and Y. S. Shen, *Sens. Actuators, B*, 1997, **40**, 161.
4 Y. Nakatari and M. Matsuoka, *Jpn. J. Appl. Phys.*, 1982, **21**, L758.
5 A. Glisenti, *J. Chem. Soc., Faraday Trans.*, 1998, **94**, 3671.
6 S. Hmada and E. Matijevic, *J. Chem. Soc. Faraday Trans*, 1982, **178**, 2147.
7 S. Hamada, S. Niizrki and Y. Kudo, *Bull. Chem. Soc. Jpn.*, 1986, **59**, 3443.
8 P. Ayyub, M. Multani, M. Barma, V. R. Palkar and R. Vijayaraghavan, *J. Phys. C: Solid State Phys.*, 1988, **21**, 2229.
9 T. Hashimoto, T. Yoko and S. Saka, *J. Ceram. Soc. Jpn.*, 1993, **101**, 64.
10 D. Dong, P. Hong and S. Dai, *Mater. Res. Bull.*, 1995, **30**, 537.
11 C. Pascal, J. L. Pascal and F. Favier, *Chem. Mater.*, 1999, **11**, 141.
12 C. Sudakar, G. N. Subbanna and T. R. N. Dutty, *J. Mater. Chem.*, 2002, **12**, 107.
13 R. M. Dell, *Reactivity of Solids*, ed. J. S. Anderson, M. W. Roberts and F. Stone, Chapman and Hall, New York, 1972, p. 553.
14 W. T. Dong, S. X. Wu and D. P. Chen, *Chem. Lett.*, 2000, **5**, 496.
15 Y. Q. Xie, *J. Am. Ceram. Soc.*, 1999, **82**(3), 768.
16 Y. Q. Xie, *Chin. J. Mater. Res.*, 2000, **14**, 45.
17 A. E. Gash, T. M. Tillotson and J. H. Satcher, *Chem. Mater.*, 2001, **13**, 999.
18 D. Sugimoto, *Adv. Colloid Interface Sci.*, 1978, **28**, 65.
19 C. M. Flynn, *Chem. Rev.*, 1984, **84**, 31.
20 K. Tuscuda, *Synthetic Reactions of Polymers*, published by niken koyou shibunshya, 1978, translated by G. W. Chen and J. S. Shen, Science Publisher, Beijing, 1983, p. 80 (in Chinese).
21 G. Odian, *Principles of Polymerization*, John Wiley & Sons, 1981, translated by H. Li, W. Q. Huang, Z. W. Gu, Science Publisher, Beijing, 1985, p. 340 (in Chinese).
22 L. D. Zhang and J. M. Mou, *Nanomaterial Science*, Liaoning Science and Technology Publisher, Shenyang, 1994, p. 94 (in Chinese).
23 B. Z. Dong, W. J. Sheng, H. L.Yang and Z. J. Zhang, *J. Appl. Crystallogr.*, 1997, **30**, 877.
24 A. R. West, *Solid State Chemistry and its Applications*, John Wiley & Sons Ltd., 1984, translated by M. Z. Su, G. Y. Xie and P. W. Shen, Fudan University Publishing House, Shanghai, 1989, p. 128 (in Chinese).
25 A. Guinier and G. Fournet, *Small Angle Scattering of X-rays*, John Wiley, New York, 1955.
26 J. A. Uuston, R. M. Richardson, S. L. Jones and C. Norman, in *Better Ceramics Through Chemistry IV*, ed. B. J. J. Zelinsky, D. E. Clark and D. R. Ulrich, *Mater. Res. Soc. Symp. Proc.*, 1990, **180**, 123.
27 J. E. Martin and A. J. Hurd, *J. Appl. Crystallogr.*, 1987, **20**, 61.
28 S. Hamada and E. Matijevic, *J. Colloid Interface Sci.*, 1981, **84**(1), 274.
29 S. Hamada and E. Matifevic, *J. Chem. Soc., Faraday Trans. 1*, 1982, **78**, 2147.
30 Y. T. Zhang, *Acta Phys.-Chim. Sin.*, 1994, **10**(1), 50.
31 K. H. Yun, *Organic Chemistry*, People's Educational Publishing House, Beijing, 1982, p. 126 (in Chinese).
32 A. Kryukov and L. V. Nazarova, *Ukr. Khim. Zh. (Russ. Ed.)*, 1963, **29**, 806.
33 P. S. Davis and D. J. Deller, *Nature*, 1966, **212**, 404.